DOI: https://doi.org/10.62985/j.huit_ojs.vol25.no6.361

EFFICIENT CURRENT STRESS REDUCTION FOR AC-MMCS IN MACHINE DRIVE SYSTEMS

Duc Dung Le, Duc Anh Tuan Nguyen, Ngo Ly Dang, Thanh Toi Le*

Ho Chi Minh City University of Industry and Trade

*Email: *toilt@huit.edu.vn*

Received: 9 December 2024; Revised: 31 March 2025; Accepted: 2 April 2025

ABSTRACT

This paper proposes a new approach for defining the average voltage of submodule (SM) capacitors in Active Cross-Connected Modular Multilevel Converters (AC-MMCs) intended for medium-voltage motor drive applications. The concept relies on allowing a larger low-frequency voltage ripple to appear on the SM capacitors by intentionally limiting the compensation of low-frequency power variations. The resulting ripple information is then used to regulate the average capacitor voltage so that its deviations remain within the required operating bounds. By doing so, the magnitude of the AC circulating current is lowered and part of the low-frequency power oscillation is suppressed. This leads to reduced current stress on the power semiconductors, inductors, and flying capacitors. Simulation has been done to confirm the effectiveness of the proposed control method.

Keywords: Active cross-connected modular multilevel converter (MMC), capacitor voltage fluctuations, medium-voltage motor drive.

1. INTRODUCTION

Modular multilevel converters (MMCs) have recently attracted significant interest due to their benefits, including modular design and scalability [1]. As a result, they have been widely applied in medium- and high-voltage systems, such as high-voltage direct current (HVDC) transmission systems [2–4], static synchronous compensators (STATCOMs) [5], and variable-speed motor drives [6–8]. Despite these advantages, a key challenge in using MMCs for variable-speed drives is the fluctuation in submodule (SM) capacitor voltage, which is proportional to the output current level and inversely proportional to the output frequency [9–11]. This issue becomes more pronounced during low-speed operations [11-13].

Numerous studies have examined different techniques for limiting the SM capacitor voltage ripple so that stable behavior can be maintained during standstill and low-speed operation [14–16]. One widely adopted method utilizes sinusoidal modulation, which introduces high-frequency common-mode voltage (CMV) along with circulating currents in the phase legs [17–19]. Although this strategy can successfully decrease the ripple of the SM capacitor voltage without disturbing the AC phase currents or the DC-link current, the resulting CMV may increase electrical stress on motor windings, potentially accelerating insulation aging and contributing to bearing failures [13–14].

To mitigate SM capacitor voltage ripple without generating CMV at the AC output, a revised converter configuration known as the active cross-connected modular multilevel converter (AC-MMC) has been proposed [16–18]. While the AC-MMC preserves the general structure of a conventional MMC, it introduces cross-connections between the midpoint nodes of both arms in each leg. During low-speed operation, these additional links help manage the power imbalance between the arms by enabling an AC circulating current. This current offsets the low-frequency power variations and thereby reduces the ripple of the SM capacitor voltage, all without introducing CMV at the AC output. Despite these advantages, the approach also leads to challenges such as higher peak device and inductor currents, increased losses, and larger inductor size requirements.

The strategy of reducing the average capacitor voltage has been previously explored for conventional MMCs and hybrid MMCs [19-21], but it has not yet been applied to AC-MMCs. In

conventional MMCs, an optimal average SM capacitor voltage selection was proposed in [19], allowing a relatively large voltage ripple on the SM capacitors as long as it remains within their permissible operating range. This approach avoids injecting high-frequency CMV or AC circulating currents, which helps lower the overall power losses of the converter. However, this approach works effectively only when the system runs at relatively high speeds (0.3–1.0 p.u.); however, the method does not meet performance needs in the 0–0.3 p.u. speed region.

To address this limitation, high-frequency CMV and AC-circulating current injection techniques have been utilized [7, 9]. These approaches help lower the AC circulating-current amplitude in the medium-speed operating range when compared with traditional control techniques [7]. However, the selection criteria for the average SM capacitor voltage remain unexplored [22]. Furthermore, in the low-speed region, the average SM capacitor voltage is constrained to remain at its nominal level, which restricts the ability to reduce the AC circulating current amplitude. Another control approach integrates the coordination of injected CMV, AC-circulating current, and average SM capacitor voltage, enabling operation at standstill and low speeds [23, 24].

This study introduces a technique for identifying the representative voltage level of the SM capacitors in an AC-MMC. By steering the AC circulating current to follow a purposely shaped reference signal, the low-frequency power imbalance in each half-arm is reduced but not entirely removed, which produces corresponding low-frequency variations in the SM capacitor voltages. These variations are then used to adjust the capacitor voltage reference so that the maximum capacitor voltage stays within the permissible boundary. With this mechanism, the allowable voltage fluctuation can exceed 20% when the average capacitor voltage is lowered. This allows the required AC circulating current to be lowered relative to standard techniques, which in turn decreases converter losses and permits the use of smaller inductors. Furthermore, the semiconductor devices experience less voltage stress because the peak SM capacitor voltage is restricted to its rated limit. The viability of the proposed method has been demonstrated using 4160-V/1-MW simulation configuration.

2. AC-MMC CIRCUIT AND OPERATION

2.1. Topology configuration

Fig. 1 illustrates the structural arrangement of a three-phase AC-MMC. Each phase leg comprises two branches: an upper branch and a lower branch. These branches are further divided into two sub-branches. The midpoint of branches in each phase leg is connected through a linking branch formed by several SMs connected together. The linking branch contains the same count of SMs as those used in each arm.

As a result, SMs having the same voltage and current ratings can be deployed uniformly across the upper, lower, and linking branches. The SMs in the linking branch are controlled to produce a high-frequency current component is generated. This high-frequency current interacts with the high-frequency voltage present in the converter branches, which contributes to significantly reducing the capacitor voltage ripple within the SMs.

2.2. Minimizing the ripple of SM capacitor voltage during low-speed operation

To suppress the voltage ripple on the SM capacitors, a high-frequency component (v_h) is injected into both half-arms along with the fundamental term ($0.5v_x$) and the DC voltage offset ($0.25V_{dc}$) [15]. As illustrated in Fig. 1, the resulting voltages of the upper and lower half-arms can be expressed as follows:

$$v_{xU1} = 0.25V_{dc} - 0.5v_x - v_h \quad (1) \qquad v_{xL1} = 0.25V_{dc} + 0.5v_x - v_h \quad (3)$$

$$v_{xU2} = 0.25V_{dc} - 0.5v_x + v_h \quad (2) \qquad v_{xL2} = 0.25V_{dc} + 0.5v_x + v_h \quad (4)$$

where v_x and v_h are:

$$v_x = V_o \cos(\omega t + \delta_x) \quad (5)$$

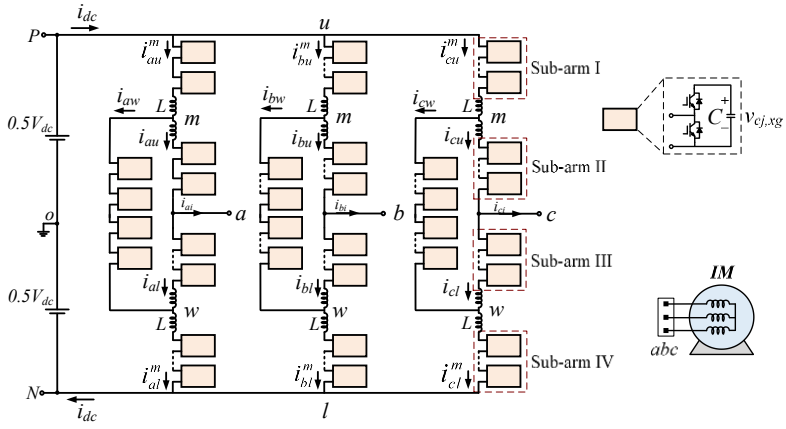

Figure 1. Circuit structure of the AC-MMC

$$v_h = V_h \cos(\omega_h t) \tag{6}$$

where V_o and V_h denote the magnitude levels of the fundamental component and the high-frequency component, respectively, ω and ω_h correspond to the angular frequencies of these two components, and δ_x is the initial phase angle. Furthermore, the expressions for the upper and lower half-arm currents are given by [15]:

$$i_{xU1} = i_{xd} + 0.5i_x + i_{xh} \tag{7}$$

$$i_{xU2} = i_{xd} + 0.5i_x - i_{xh} \tag{8}$$

$$i_{xL1} = i_{xd} - 0.5i_x - i_{xh} \tag{9}$$

$$i_{xL2} = i_{xd} - 0.5i_x + i_{xh} \tag{10}$$

The expressions for i_x and i_{xh} are as follows:

$$i_x = I_o \cos(\omega t + \delta_x - \phi) \tag{11}$$

$$i_{xh} = I_{xh} \cos(\omega_h t) \tag{12}$$

where I_o and I_{xh} denote the magnitude values, and ϕ specifies the phase shift between the voltage and current waveforms. For stable regulation of the AC circulating current, the high-frequency component (f_h) is typically limited to no more than one-tenth of the carrier frequency, f_c [8]. Using (1) and (7), the instantaneous power, p_{xU1}, associated with the upper arm's top half-arm is obtained as follows:

$$\begin{aligned} p_{xU1} = {} & 0.25V_{dc}i_{xd} - 0.25v_x i_x + 0.125V_{dc}i_x - 0.5v_x i_{xd} \\ & - 0.5V_h I_{xh} - 0.5V_h I_{xh} \cos(2\omega_h t) \end{aligned} \tag{13}$$

The first two terms on the right-hand side of (13) become equal due to the power equilibrium maintained between the DC source and the AC output. Therefore, i_{xd} is expressed as:

$$i_{xd} = \frac{v_x i_x}{V_{dc}} \tag{14}$$

When (14) is inserted into (13), the magnitude of the fourth term on the right-hand side becomes insignificant relative to the third term. Consequently, p_{xU1} contains only AC elements and may be rewritten in the following form:

$$p_{xU1} = p_{xU1} = 0.125V_{dc}i_x - 0.5V_h I_{xh} - 0.5V_h I_{xh} \cos(2\omega_h t) \tag{15}$$

The first term on the right-hand side of (15) predominantly causes the pronounced power variation that occurs at low fundamental frequencies, which in turn produces considerable ripple in the SM capacitor voltage, Δv_{sm}. To mitigate Δv_{sm}, the second term acts to offset these substantial power variations by controlling the AC circulating current, i_{xh}, so that it tracks a defined reference:

$$i_{xh}^{*} = I_{xh}\cos(\omega_h t) = \frac{V_{dc} i_x}{4V_h}\cos(\omega_h t) \tag{16}$$

As a result, only the third term on the right side of (15) continues to appear in the half-arm, causing the SM capacitors to undergo rapid charging and discharging over a brief period, thereby significantly reducing Δv_{sm}. Fig. 2(a) shows the associated circuit variables, with $\tilde{e}_{xU1}$ denoting the energy variation derived by integrating $\tilde{p}_{xU1}$ in (15). The figure indicates that the SM capacitor voltage stays close to its rated level while keeping Δv_{sm} very small.

From (7)–(10) and (16), it can be seen that under low-speed conditions, the peak half-arm current is determined by the magnitudes of i_{xd}, i_x, and i_{xh}. Because the maximum magnetic flux in the half-arm inductor core scales with its peak current [8], lowering this current is essential for reducing the inductor's physical footprint and associated losses. Therefore, limiting the contribution of i_{xh} plays an important role in reducing current-related stress. To keep the SM capacitor voltage within the permissible range, the average capacitor voltage, $v_{c,avg}$, is controlled so it does not exceed the rated value $v_{c,rated}$, defined as $V_{dc/N}$ (where N denotes the number of SMs assigned to each arm).

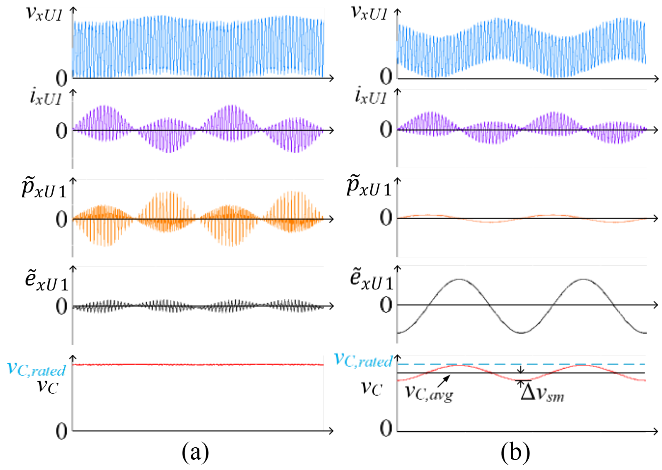

Figure 2. Evaluation of circuit-related quantities in an FC-MMC during low-speed operation
(a) Existing approach (b) Proposed method

3. PROPOSED METHOD

To decrease the amplitude of i_{xh}, the average capacitor voltage must be set below the rated value, $v_{c,rated}$. However, selecting an appropriate $v_{c,avg}$ is constrained by several practical considerations. When the average capacitor voltage is reduced, the achievable output-voltage amplitude is also lowered, which can adversely affect the converter's operating capability and overall system performance.

3.1. Determination of average capacitor voltage ($v_{c,avg}$) range

To reduce the influence of the low-frequency power variation in (15) (i.e., the first term on the right-hand side), the second term is regulated so that it scales with the low-frequency power component:

$$0.5 V_h I_{xh} = \alpha \cdot 0.125 V_{dc} i_x \tag{17}$$

where α is a tuning factor that specifies how much of the low-frequency power fluctuation is compensated, taking values between zero and one. When $\alpha = 1$, the low-frequency power variation is entirely eliminated. Under this condition, the SM capacitor voltage ripple is fully removed—analogous to the conventional approach [15], but the voltage reference is set to $v_{c,avg}$ rather than $v_{c,rated}$. When $\alpha = 0$, injecting the high-frequency components (v_h and i_{xh}) provides no mitigation effect. The high-frequency power term (the third component on the right-hand side of (15)) becomes insignificant because its contribution to the low-frequency power variation is minimal. From (17), the reference expression for the AC circulating current i_{xh}^{*}, is obtained as:

$$i_{xh}^{*} = \alpha I_{xh}\cos(\omega_h t) = \alpha \frac{V_{dc} i_x}{4V_h}\cos(\omega_h t) \tag{18}$$

It is worth mentioning that a square-wave approach may also be used, where shaping the injected high-frequency waveform can lower the peak magnitude of i_{xh} to a certain degree [17]. For ease of analytical development, the proposed strategy adopts a sinusoidal waveform for the high-frequency component. By inserting (11) and (17) into (15), the residual low-frequency power term in the upper branch's top half-arm after compensation can be expressed as:

$$p_{xU1} = \frac{(1-\alpha)}{8} V_{dc} I_o \cos(\omega t + \delta_x - \phi) \tag{19}$$

Figure 2(b) presents the waveform of p_{xU1} which indicates that a portion of the low-frequency power variation still remains after compensation. By performing the integration in (19), the corresponding energy fluctuation ($\tilde{e}_{xU1}$) can be expressed as:

$$\tilde{e}_{xU1} = \frac{(1-\alpha)}{8\omega} V_{dc} I_o \sin(\omega t + \delta_x - \phi) \tag{20}$$

As illustrated in Fig. 2(b), the peak-to-peak energy variation of the half-arm given in (20) can be written as:

$$\Delta\tilde{e}_{xU1\_PP} = \frac{(1-\alpha)}{4\omega} V_{dc} I_o \tag{21}$$

In the half-arm, the SM capacitor voltages and the corresponding energy variation, $\Delta\tilde{e}_{xU1\_pp}$, are linked through the following mathematical relation:

$$\Delta\tilde{e}_{xU1\_PP} = \frac{N}{2}\left(\frac{1}{2}C\left(v_{c,avg} + \Delta v_{sm}\right)^2 - \frac{1}{2}C\left(v_{c,avg} - \Delta v_{sm}\right)^2\right) \tag{22}$$

Δv_{sm} is obtained from (21) and (22) as follows:

$$\Delta v_{sm} = \frac{(1-\alpha) V_{dc} I_o}{4\omega N C v_{c,avg}} \tag{23}$$

The magnitude of Δv_{sm} shown in Fig. 2(b) exceeds the value obtained using the conventional method depicted in Fig. 2(a) since the low-frequency power variation is significantly diminished. As a result, the maximum SM capacitor voltage must be limited. The maximum limit of the SM capacitor in the suggested technique is the rated voltage, $v_{c,rated}$, which is connected to $v_{c,avg}$, and Δv_{sm} in the following ways:

$$v_{c,avg} + \Delta v_{sm} \le v_{c,rated} \tag{24}$$

Putting (23) in place of (24),

$$\left(v_{c,avg}\right)^2 - v_{c,rated} v_{c,avg} + \frac{(1-\alpha) V_{dc} I_o}{4\omega N C} \le 0 \tag{25}$$

The quadratic inequality's discriminant, D, in (25) can be written as follows:

$$D = \left(v_{c,rated}\right)^2 - \frac{(1-\alpha) V_{dc} I_o}{\omega N C} \tag{26}$$

D should not be negative to get the true roots, from which:

$$\left(v_{c,rated}\right)^2 \ge \frac{(1-\alpha) V_{dc} I_o}{\omega N C} \tag{27}$$

The coefficient α should meet the following requirement based on (27).

$$\alpha \geq 1 - \frac{v_{c,rated}\omega C}{I_o} \tag{28}$$

The range of $v_{c,avg}$ can be derived as follows with the lowest limit of α:

$$\frac{v_{c,rated} - \sqrt{D}}{2} \leq v_{c,avg} \leq \frac{v_{c,rated} + \sqrt{D}}{2} \tag{29}$$

In order to maximize the quantity of energy storage in the converter, the upper limit in (29) is taken as a reference value of $v_{c,avg}$. Furthermore, (28) shows that at very low speeds, the coefficient α is almost equivalent to one. On the other hand, the coefficient decreases as the operating speed increases. A speed threshold, ω_{th}, at $\alpha = 0$ can be computed using (28), as follows:

$$\omega_{th} = \frac{I_o}{v_c^{rated} C} \tag{30}$$

This indicates that the injection of high-frequency components can reduce the low-frequency power variation and the associated ripple in the SM capacitor voltage if $\omega \leq \omega_{th}$. Based on the coefficient α, the upper limit of $v_{c,avg}$ in (29) is chosen for this operating speed range in order to meet the limitation in (24). On the other hand, alleviation is impossible if the operating speed is high enough above the threshold ($\omega > \omega_{th}$), and a zero value of α is used to choose the maximum limit of $v_{c,avg}$. Here, the two half-arm currents in one arm are the same, and the AC-MMC is operated similarly to a traditional MMC [15].

3.2. Determination of $v_{c,avg}$ and α

Figure 3 provides a flowchart of the proposed control method, outlining the procedure used to compute $v_{c,avg}^{*}$ are illustrated. The first step checks whether low-frequency power variations can be attenuated by comparing ω and ω_{th}. If mitigation is achievable, α is set to the minimum level specified in (28). If $\alpha = 0$, the value of v_{c,avg_1} is obtained using the discriminant, D.

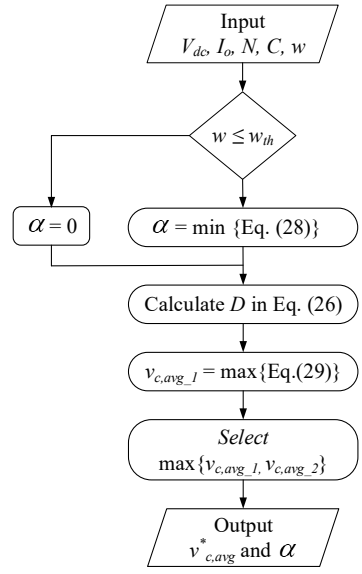

Figure 3. Flowchart of the proposed control method

3.3. Control algorithm

Fig. 4 provides the block diagrams that outline the proposed control method. The leg-balancing controller illustrated in Fig. 4(a) adjusts the mean capacitor voltage for the SMs in phase-x so that it tracks the commanded value $v_{c,avg}^{*}$. $v_{c,x}^{avg}$ is expressed as follows:

$$v_{c,x}^{avg} = \frac{1}{2N}\sum_{j=1}^{N}\left(v_{cj,xU} + v_{cj,xL}\right) \tag{31}$$

where $v_{cj,xU}$ and $v_{cj,xL}$ represent the capacitor voltages of the j-th submodule in the upper and lower arms. The outer voltage controller provides the reference signal for the inner DC-circulating current control loop, i_{xd}^{*}. Consequently, this produces the compensating phase-voltage command $\Delta v_{ph,x}^{*}$.

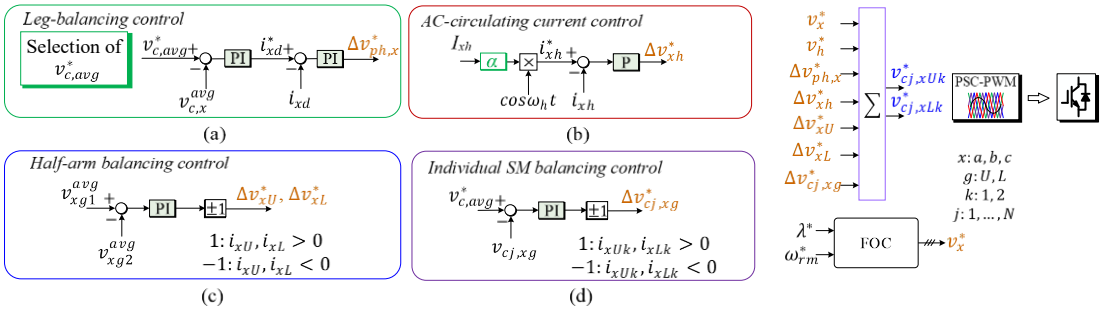

Figure 4. Block diagram of the newly proposed method. (a) Leg-balancing control. (b) Control of AC-circulating current. (c) Half-arm balancing control. (d) Individual SM balancing control.

Figure 4(b) illustrates the AC-circulating current controller, in which i_{xh} is regulated to track its reference value i_{xh}^{*}. The magnitude of the reference of i_{xh}^{*} is tuned through the parameter α. In contrast to the method described in [15], the proposed approach streamlines the structure by eliminating the voltage-control stage. The output of the AC-circulating regulator generates the voltage command, Δv_{xh}^{*}. Fig. 4(c) shows the half-arm balancing controller, aimed at balancing the mean SM-capacitor voltages between the top and bottom half-arms of the same phase arm (v_{xg1}^{avg} and v_{xg2}^{avg}, where $g = \{U, L\}$ denotes both arms). Its output generates the compensating half-arm voltage signals Δv_{xU}^{*} and Δv_{xL}^{*}.

Fig. 4(d) presents the individual SM-balancing controller, which ensures that the voltage of every SM capacitor tracks the reference value $v_{c,avg}^{*}$. The controller outputs the compensating voltage command for each submodule, $\Delta v_{cj,xg}^{*}$. As a result, the voltage commands issued to the SMs in the upper and lower arms ($v_{cj,xUk}^{*}$ and $v_{cj,xLk}^{*}$, where $k = \{1, 2\}$ corresponds to the top and bottom half-arms) are as follows:

$$v_{cj,xUk}^{*} = v_{c,rated} - 0.5v_{c,avg}^{*} - \frac{v_x^{*}}{N} \mp \frac{2v_h^{*}}{N} - \Delta v_{ph,x}^{*} \mp \Delta v_{xh}^{*} \mp \Delta v_{xU}^{*} + \Delta v_{cj,xg}^{*} \tag{32}$$

$$v_{cj,xLk}^{*} = v_{c,rated} - 0.5v_{c,avg}^{*} + \frac{v_x^{*}}{N} \mp \frac{2v_h^{*}}{N} - \Delta v_{ph,x}^{*} \mp \Delta v_{xh}^{*} \mp \Delta v_{xL}^{*} + \Delta v_{cj,xg}^{*} \tag{33}$$

v_h^{*}, can be defined follows:

$$v_h^{*} = \left(0.25Nv_{c,avg}^{*} - 0.5V_0\right)\cos\left(\omega_h t\right) \tag{34}$$

4. SIMULATION RESULTS

To evaluate the effectiveness of proposed control strategy, simulation tests were performed by using PSIM software on a 4160-V/1-MW AC-MMC-based IM drive system featuring four SMs per arm. The parameters of the converter and induction motor (IM) used for simulation are listed in Tables 1 and 2, respectively.

Table 1. Parameters of MMC used for simulation

Parameters	Values
Rated apparent output (S)	1.081 (MVA)
DC-link potential (V_{dc})	7 (kV)
Number of SMs per arm (N)	4
Inductance value of a single half-arm (L)	2.5 (mH)
Nominal voltage rating of each SM (v_C^*)	1.75 (kV)
Capacitance value of the SM capacitor (C)	2700 (μF)
Switching carrier frequence (f_c)	2 (kHz)
Injected high-frequence component (f_h)	180 (Hz)

Table 2. Parameters of IM used for simulation

Parameters	Values
Rated power (P_o)	1250 (hp)
Rated line-to-line voltage (V_{ll})	4.16 (kV)
Rated operating current (I_{rated})	150 (A)
Rated electrical frequency (f_o)	60 (Hz)
Rated mechanical speed (ω_{rm_rated})	1189 (rpm)
Rated torque output (T_{rated})	7.49 (kN.m)

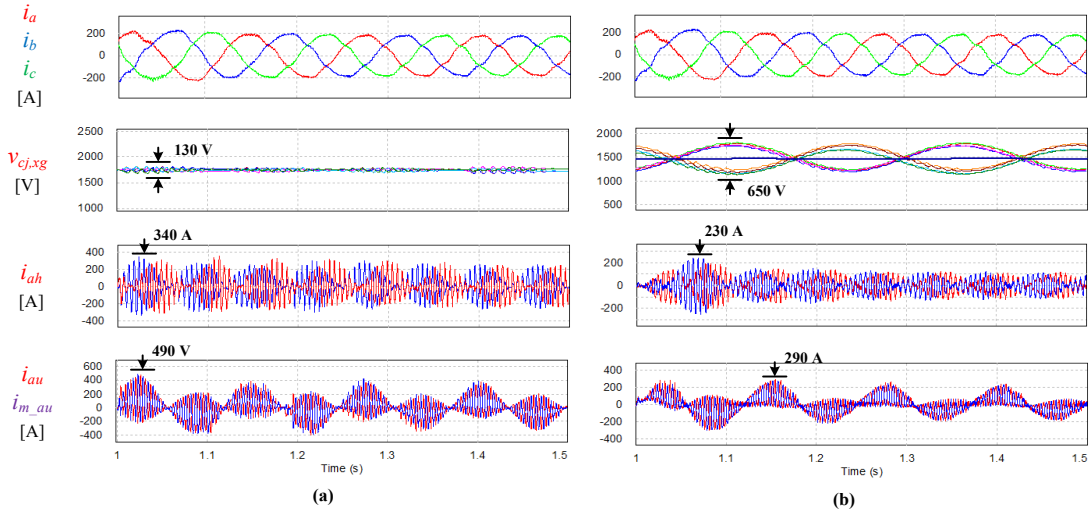

Figure 5. Operating performance of the AC-MMC at a mechanical speed of 150 rpm under full-load operation. (a) Existing control approach. (b) Newly proposed control approach.

Fig. 5 presents the operating behavior of the AC-MMC using both the conventional and the proposed control methods at a mechanical speed of 150 rpm under full-load conditions. The root mean square (RMS) value of the three-phase output currents is 150 A and and the fundamental frequency (f_o) is 5 Hz. Fig. 5(a) shows the performance obtained with the conventional approach, which completely suppresses low-frequency power oscillations. Under this method, the SM capacitor voltages remain well regulated around the rated level $v_{c,rated}$ = 1750 V, with a voltage ripple of approximately Δv_{sm} = 130 V. Fig. 5(b) illustrates the results with the proposed strategy for α = 0.6. In this case, the SM capacitor voltages are regulated to track a reference of $v_{c,avg}^*$ 1468 V, and the peak values reach about 1793 V. These peaks are slightly higher than $v_{c,rated}$, primarily due to the small terms appearing in (13). Under the conventional control, the peak values of the AC-circulating current (i_{ah}) and the upper arm

currents (i_{aU1} and i_{aU2}) are 340 A and 490 A, respectively. With the proposed method, these peak currents are reduced to 230 A and 290 A. As a result, the electrical stress experienced by the switching devices and inductors decreases by roughly 40% compared with the traditional approach.

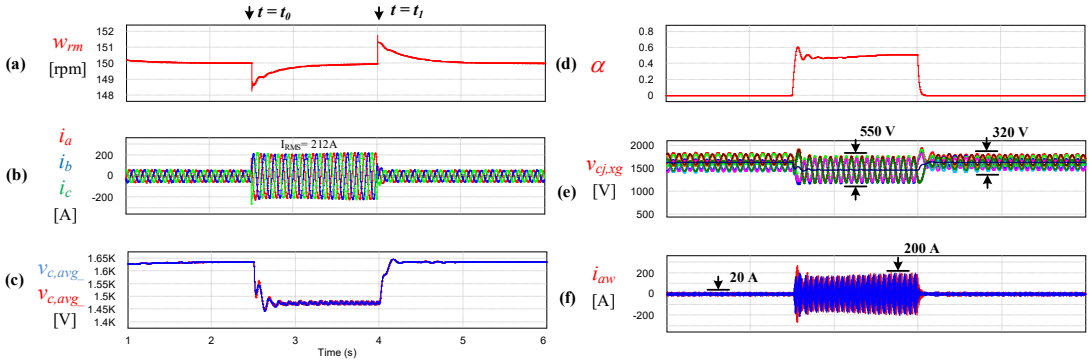

Figure 6. Performance of AC-MMC at ω_{rm} = 150 rpm under load change condition.
(a) Motor speed (b) 3-phase output current (c) Average capacitor voltage
(d) The Coefficient α (e) Upper branch submodule capacitor voltage (f) Circulating current

The mechanical speed at ω_{rm} = 150 rpm is illustrated in Fig. 6(a), where the load increases from no-load to full-load at t_0, and the load decreases back to its initial state at t_1. The motor input current is demonstrated in Fig. 6(b). Fig. 6(c) illustrates the average capacitor voltage, which remains stable at 1635V during no-load operation and drops to 1475V when increasing to full-load operation. With α = 0, the capacitor voltage of the sub-modules is controlled at the reference level of 1635V, with fluctuations around 320V. When the load changes and α = 0.6, the capacitor voltage of the SMs is controlled at the reference level of 1475V, and the fluctuations increase to 550V, as shown in Fig. 6(d) and 6(e). It can be observed that the average capacitor voltage and its fluctuation remain stable. The peak voltage is approximately 1795V, indicating that the maximum capacitor voltage is maintained below 110% of the rated value $v_{c,rated}$ (1750V × 1.1). Fig. 6(f) shows the circulating AC current (i_{ah}) with a peak value of 20 A, during no-load condition. At the time of load variation, the peak value increases to 200A.

5. CONCLUSION

This work proposes a new approach for determining the average capacitor voltage of the submodules (SMs) in an AC-MMC. Instead of completely cancelling the low-frequency power variation in each half-arm, the method intentionally allows a controlled amount of this fluctuation to remain, which produces a predictable low-frequency voltage ripple on the SM capacitors. This ripple serves as the basis for computing an appropriate average capacitor voltage over a range of operating conditions, ensuring that the SM capacitor voltages stay within the permissible range. Since the low-frequency power component is only partially suppressed, the amplitude of the AC circulating current is also reduced. The feasibility and performance of the proposed control scheme are demonstrated through simulations using a 4160-V/1-MW model.

REFERENCES

1. Lesnicar A., & Marquardt R. - An innovative modular multilevel converter topology suitable for a wide power range. 2003 IEEE Bologna Power Tech Conference Proceedings **3** (2003) 6. https://doi.org/10.1109/PTC.2003.1304403
2. Allebrod S., Hamerski R., & Marquardt R. - New transformerless, scalable Modular Multilevel Converters for HVDC-transmission. 2008 IEEE Power Electronics Specialists Conference (2008) 174-179. https://doi.org/10.1109/PESC.2008.4591920
3. Solas E., Abad G., Barrena J.A., Aurtenetxea S., Carcar A., and Zajac L. - Modular multilevel converter with different submodule concepts-part II: Experimental validation and comparison for

HVDC application. IEEE Trans. Ind. Electron. **60** (10) (2013) 4536-4545. https://doi.org/10.1109/TIE.2012.2211431

4. Jo Y.J., Nguyen T.H., and Lee D.C. - Capacitance estimation of the submodule capacitors in modular multilevel converters for HVDC applications. J. Power Electron. **16** (5) (2016) 1752–1762. http://doi.org/10.6113/JPE.2016.16.5.1752
5. Peng F. Z., J. Lai, Mckeever J. W., and Vancoevering J. - A multilevel voltage-source inverter with separate DC sources for static var generation. IEEE Trans. Ind. Appl. **32** (5) (1996) 1130–1138. http://doi.org/10.1109/IAS.1995.530626
6. Hagiwara M., Nishimura K., and Akagi H. - A medium-voltage motor drive with a modular multilevel PWM inverter. IEEE Trans. Power Electron. **25** (7) (2010) 1786–1799. http://doi.org/10.1109/TPEL.2010.2042303
7. Korn A. J., Winkelnkemper M., and Steimer P. - Low output frequency operation of the modular multi-level converter. Proc. IEEE ECCE, 2010, pp. 3993–3997. http://doi.org/10.1109/ECCE.2010.5617802
8. Hagiwara M., Hasegawa I., and Akagi H. - Start-up and low-speed operation of an electric motor driven by a modular multilevel cascade inverter. IEEE Trans. Ind. Appl. **49** (4) (2013) 1556–1565. http://doi.org/10.1109/TIA.2013.2256331
9. Antonopoulos A., Ängquist L., Norrga S., Ilves K., and Nee H. P. - Modular multilevel converter AC motor drives with constant torque from zero to nominal speed. IEEE Trans. Ind. Appl. **50** (3) (2012) 739-746. http://doi.org/10.1109/ECCE.2012.6342746
10. Picas R., Zaragoza J., Pou J., Ceballos S., Konstantinou G., and Capella G. J. - Study and comparison of discontinuous modulation for modular multilevel converters in motor drive applications. IEEE Trans. Ind. Electron. **66** (3) (2019) 2376–2386. http://doi.org/10.1109/TIE.2018.2847621
11. Debnath S., Qin J., and Saeedifard M. - Control and stability analysis of modular multilevel converter under low-frequency operation. IEEE Trans. Ind. Electron. **62** (9) (2015) 5329–5339. http://doi.org/10.1109/TIE.2015.2414908
12. Espinoza M., Cárdenas R., Díaz M., and Clare J. C. - An enhanced dq-based vector control system for modular multilevel converters feeding variable-speed drives. IEEE Trans. Ind. Electron. **64** (4) (2017) 2620–2630. http://doi.org/10.1109/TIE.2016.2637894
13. Li B. et al. - An improved circulating current injection method for modular multilevel converters in variable-speed drives. IEEE Trans. Ind. Electron. **63** (11) (2016) 7215–7225. http://doi.org/10.1109/TIE.2016.2547899
14. Zhao F., Xiao G., Zhu T., Zheng X., Wu Z., and Zhao T. - A coordinated strategy of low-speed and start-up operation for medium-voltage variable-speed drives with a modular multilevel converter. IEEE Trans. Power Electron., vol. **35**, no. 1, pp. 709–724, 2020. http://doi.org/10.1109/TPEL.2019.2913696
15. Du S., Wu B., Zargari N. R., and Cheng Z. - A flying-capacitor modular multilevel converter for medium-voltage motor drive. IEEE Trans. Power Electron. **32** (3) (2017) 2081–2089. http://doi.org/10.1109/TPEL.2016.2565510
16. Le D.D., Lee D.C., and Kim H.G. - Three-phase flying-capacitor MMC with six coupled inductors. J. Power Electron. **20** (4) (2020) 916-925. http://doi.org/10.1007/s43236-020-00099-3
17. Du S., Wu B., and Zargari N.R. - Current stress reduction for flying-capacitor modular multilevel converter. IEEE Trans. Power Electron. **34** (1) (2019) 184–191. http://doi.org/10.1109/TPEL.2018.2827947
18. Le D.D. and Lee D.C. - Reduction of half-arm current stresses and flying-capacitor voltage ripples of flying-capacitor MMCs. IEEE Access **8** (2020) 180076–180086. http://doi.org/10.1109/ACCESS.2020.3027844
19. Antonopoulos A., Ängquist L., Harnefors L., and Nee H.P. - Optimal selection of the average capacitor voltage for variable-speed drives with modular multilevel converters. IEEE Trans. Power Electron. **30** (1) (2022) 227–234. http://doi.org/10.1109/TPEL.2014.2316273.

20. Zhou S., Li B., Guan M., Zhang X., Xu Z., and Xu D. - Capacitance reduction of the hybrid modular multilevel converter by decreasing average capacitor voltage in variable-speed drives. IEEE Trans. Power Electron. **34** (2) (2019) 1580-1594. http://doi.org/10.1109/TPEL.2018.2833503
21. Antonopoulos A., Ängquist L., and Nee H.P. - On dynamics and voltage control of the modular multilevel converter. Proc. 13th ECPE Europe, 2009, pp. 1–10.
22. Ilves K., Norrga S., Harnefors L., and Nee H.P. - On energy storage requirements in modular multilevel converters. IEEE Trans. Power Electron. **29** (1) (2014) 77–88. http://doi.org/10.1109/TPEL.2013.2254129
23. Le D.D., Lee D.C, and Nho E.C. - Fault-tolerant capability of MMC with novel structure of middle submodules. J. Power Electron. **23** (2023) 1342–1352. http://doi.org/10.1007/s43236-023-00679-z
24. Gui Q., Fehr H., and Gensior A. - Energy Control of Modular Multilevel Converters for Drive Applications at Low Frequency Using General Averaging - IEEE Transactions on Power Electronics **39** (5) (2024) 5239-5256. http://doi.org/10.1109/TPEL.2024.3360000.

TÓM TẮT

PHƯƠNG PHÁP GIẢM DÒNG ĐIỆN TUẦN HOÀN CHO BỘ BIẾN ĐỔI ĐA BẬC CẤU HÌNH LIÊN KẾT MÔ-ĐUN ỨNG DỤNG CHO HỆ TRUYỀN ĐỘNG MÁY

Lê Đức Dũng, Nguyễn Đức Anh Tuấn, Đặng Ngô Lý, Lê Thành Tới*

Trường Đại học Công Thương Thành phố Hồ Chí Minh

*Email: *toilt@huit.edu.vn*

Nghiên cứu này giới thiệu một phương pháp tính toán điện áp trung bình của tụ điện mô-đun (SM), nhằm mục đích giảm thiểu áp lực dòng điện trong các bộ biến đổi đa bậc cấu hình liên kết mô-đun (AC-MMCs) được sử dụng cho hệ thống điều khiển động cơ xoay chiều trung thế. Phương pháp này bao gồm việc tạo ra các dao động điện áp tần số thấp trong tụ điện SM bằng cách giảm công suất với tần số thấp. Dựa vào giá trị dao động này, điện áp trung bình của tụ điện SM được điều chỉnh để đảm bảo các dao động của nó nằm trong giới hạn chấp nhận được. Kết quả là biên độ của dòng điện xoay chiều tuần hoàn được giảm, góp phần làm giảm một phần dao động công suất tần số thấp. Điều này giúp giảm áp lực dòng điện trong các thiết bị đóng cắt, cuộn cảm và tụ điện. Hiệu quả của phương pháp đề xuất đã được xác minh thông qua các kết quả mô phỏng.

Từ khóa: Dòng điện nhánh, hệ thống điều khiển động cơ trung thế, bộ chuyển đổi đa bậc mô-đun (MMC), dao động điện áp tụ điện mô-đun (SM).